Cite as: T. H. Prettyman *et al.*, *Science* 10.1126/science.aah6765 (2016).

Extensive water ice within Ceres' aqueously altered regolith: Evidence from nuclear spectroscopy

T. H. Prettyman,[1]* N. Yamashita,[1] M. J. Toplis,[2] H. Y. McSween,[3] N. Schorghofer,[4] S. Marchi,[5] W. C. Feldman,[1] J. Castillo-Rogez,[6] O. Forni,[2] D. J. Lawrence,[7] E. Ammannito,[8] B. L. Ehlmann,[6,9] H. G. Sizemore,[1] S. P. Joy,[8] C. A. Polanskey,[6] M. D. Rayman,[6] C. A. Raymond,[6] C. T. Russell[8]

[1]Planetary Science Institute, 1700 East Fort Lowell, Suite 106, Tucson, AZ 85719-2395, USA. [2]Institut de Recherche d'Astrophysique et Planétologie, Centre National de la Recherche Scientifique, Université Paul Sabatier, Toulouse, France 31400. [3]Department of Earth and Planetary Sciences, University of Tennessee, Knoxville, TN 37996-1410, USA. [4]University of Hawaii, 2680 Woodlawn Drive, Honolulu, HI 96822, USA. [5]Southwest Research Institute, Boulder, CO 80302, USA. [6]Jet Propulsion Laboratory, California Institute of Technology, Pasadena, CA 91109-8099, USA. [7]Johns Hopkins University, Applied Physics Laboratory, Laurel, MD 20723, USA. [8]Earth Planetary and Space Sciences, University of California, Los Angeles, Los Angeles, CA 90095-1567, USA. [9]Division of Geological and Planetary Sciences, California Institute of Technology, Pasadena, CA 91125, USA.

***Corresponding author. Email: prettyman@psi.edu**

The surface elemental composition of dwarf planet Ceres constrains its regolith ice content, aqueous alteration processes, and interior evolution. Using nuclear spectroscopy data acquired by NASA's Dawn mission, we determined the concentrations of H, Fe, and K on Ceres. The data show that surface materials were processed by the action of water within the interior. The non-icy portion of Ceres' C-bearing regolith contains similar amounts of H to aqueously altered carbonaceous chondrites, but less Fe. This allows for the possibility that Ceres experienced modest ice-rock fractionation, resulting in differences between surface and bulk composition. At mid-to-high latitudes, the regolith contains high concentrations of H, consistent with broad expanses of water ice, confirming theoretical predictions that ice can survive for billions of years just beneath the surface.

With a measured bulk density between ice and rock, dwarf planet Ceres is expected to be volatile rich, with about 17-30 wt.% water ice (*1*, *2*). Internal heating generated by the decay of radioactive elements may have driven aqueous alteration and differentiation to form a rocky interior and icy outer shell (*3*, *4*). Orbital measurements by Dawn's Visible and Infrared Mapping Spectrometer (VIR) show that Ceres' global surface contains aqueous alteration products: ammoniated clays, serpentine, and carbonates (*1*). Localized deposits of surficial water ice, while present, are rare (*5*); however, the high-latitude surface is sufficiently cold that water ice can survive within a meter of the surface over Ceres' 4.5 Ga lifetime (*6*). Physical differentiation allowed by gravity measurements (*7*) may have resulted in chemical fractionation, with surface regions that are not compositionally representative of the bulk. We refer to this style of differentiation as "ice-rock fractionation," which can be tested by comparing the composition of Ceres' surface to CI and CM carbonaceous chondrites. Although often invoked as analogs for Ceres [e.g., (*1*)], these primitive meteorites likely experienced isochemical aqueous alteration on smaller parent bodies (*8*).

NASA's Dawn mission aimed to map the chemical composition of Ceres' uppermost regolith, providing constraints on origins and evolution. In December 2015, the Dawn spacecraft entered a circular polar, low-altitude mapping orbit (LAMO), with a mean altitude of 0.82 Ceres body radii. In LAMO, Dawn's Gamma Ray and Neutron Detector (GRaND) (*9*) is sensitive to elemental composition. GRaND measures gamma rays and neutrons produced by the steady interaction of galactic cosmic rays and gamma rays from the decay of radioelements within a few decimeters of the surface. Elemental analyses presented here use data accumulated over five months in LAMO.

Maps of neutron and gamma ray counting rates, corrected for temporal changes in galactic cosmic ray flux and measurement geometry (*10*), reveal spatial variations in surface elemental composition (Fig. 1). The rate of ^{6}Li(n,α) reactions in GRaND's lithium-loaded glass (LiG) scintillator depends on the flux of thermal and epithermal neutrons, which varies inversely with regolith H content. Neutron capture by Fe in Ceres' regolith produces a gamma-ray doublet at 7.6 MeV. These signatures vary strongly with latitude, with counts decreasing toward the poles. Longitude variations are comparatively small. The dynamic range of the composition data is larger than measured by GRaND at Vesta (*11*).

In Fig. 2, mapped counting data were normalized to globally-averaged measurements of Vesta and compared with models of analog materials. On Ceres, hydrogen is predominantly in the form of water ice and hydrated minerals (*1*, *5*, *12*). Consequently, we simulated changes in the hydra-

tion state of regolith materials by adding/removing hydrogen in the form of water to/from model compositions. This allows hydrogen concentration to be expressed in terms of water equivalent hydrogen (WEH). The regolith was modeled as a two-layer structure, with an ice-free upper layer covering icy soil (Fig. 2, inset), consistent with ice stability models (*13*). Both layers have the same non-icy composition, with the lower layer containing an additional, variable fraction of water ice.

Figure 2 shows simulated hydration trends for selected materials with different Fe concentrations. Their arched shape results from an initial increase in the low-energy neutron population with small amounts of added hydrogen, which enhances capture gamma ray production, followed by a decrease in gamma production as Fe is diluted by water. With layering, the model counts deviate from the hydration trends, following different paths between non-layered end-members as depth is varied. For each material, there is a corresponding set of counts spanned by permutations of hydration and layering.

For comparison with the models, Ceres measurements were normalized to globally-averaged counting rates for Vesta. The vestan measurements were further normalized to a model, in which Vesta's global regolith composition was assumed to be similar to the howardite meteorites with the addition of 250 μg/g H, the lower bound determined by GRaND at Vesta (*11*). In this case, Ceres data plot inside the layered set for the CI and CM model compositions. Furthermore, the data points form a concave up pattern, consistent with trends for layering. If Vesta's regolith contained more H, the data points for Ceres would shift toward the hydration trends for the CI and CM chondrites; however, the lower bound is our best estimate given most of the H was delivered to Vesta by carbonaceous chondrite impactors, as detailed in (*10*).

Near the equator and within GRaND's field of view, stability models predict that water ice is at depths greater than sensed by GRaND (Fig. 3, B and C). Consequently, hydration trends describe the equatorial measurements (e.g., yellow points in Fig. 2). That these do not follow a specific hydration curve indicates that [Fe] is variable at the equator (square brackets denote concentration). Since the hydration trends for CI and CM do not intersect the data points, they can be excluded as representative compositions. For Ceres, the maximum equatorial points are consistent with simulated material E1 (*10*), which is poorer in Fe than the average CI chondrite.

By adopting the minimum value for Vesta's global average [H] and ignoring layering, [H] can be mapped as a lower bound (*14*). The spatial variation of H on Ceres can be estimated with a total uncertainty of less than 1 wt.% WEH from thermal + epithermal neutron rates (*10*). The resulting map of [H] varies strongly with latitude and is asymmetric, with higher [H] in the north than the south (Fig. 3A). The difference between the poles (2.5 ± 1.1 wt.% WEH) is larger than predicted by ice stability models given Ceres' precessing orbital elements. Epithermal and fast neutron maps are also asymmetrical (*10*), which implies subtle differences in composition and/or layering between the two hemispheres.

Based on forward modeling of zonally-averaged thermal + epithermal counting rates (*10*), water ice approaches the surface above about 40° latitude in both hemispheres (Fig. 3). The spatial distribution of OH and ammoniated phyllosilicates measured by VIR at up to 60° latitude is relatively uniform (*12*). Thus, the latitude variation of GRaND measurements is not likely due to changes in abundance or hydration state of minerals within the uppermost surface layer. An estimate of [H] in the ice table can be obtained by subtracting the equatorial [H] from the values measured at the poles. Using this approach, we find that Ceres' ice table contains at about 10 wt.% water ice, given the ice table is within a cm of the surface at the poles (Fig. 3B). The calculated porosity of the regolith is 0.2, assuming the ice fills the pores and the grain density is 2.5 g/cm^3, representative of CI and CM chondrites (*15*).

Water vapor diffusivity and soil thermal properties determine where the ice table approaches the surface within depths sensed by GRaND. The diffusion coefficient scales with grain size and porosity (*13*). Figure 3B shows ice table depths 4.5 Ga after formation, calculated for two cases considered by (*6*): a grain size of 1 μm and porosity of 0.1 (low diffusivity, Case a); and a grain size of 10 μm and porosity of 0.5 (high diffusivity, Case b). A third case representing our lower bound porosity of 0.2, with 1 μm grain size is also shown (low diffusivity, Case c), which gives a similar latitude depth profile to Case a. Forward models of thermal + epithermal counts are compared with the data in Fig. 3C. The low diffusivity Case c most closely matches the data.

The steady-state water vapor emission rate implied by the models (0.003 kg/s for case c) is much lower than the 6 kg/s inferred from Herschel Space Observatory data (*16*). Sublimation of subsurface ice can neither explain the episodic emissions observed by the Herschel Telescope nor a possible transient atmosphere observed by Dawn/GRaND during the Survey orbit mission phase (*17*). Hence, the Herschel observations may relate to the temporary exposure of ice on the surface.

Measurements of H and Fe provide constraints on the abundance of aqueous alteration products, assuming the mineralogy is similar to carbonaceous chondrites (*10*). The average equatorial [H] of 17 ± 2 wt.% WEH, which is representative of Ceres non-icy regolith, is similar to measured upper limits for CM and CI chondrites of about 14% WEH (*18*). These meteorites contain up to a few weight percent

organic material, with a H/C ratio of about 0.7 (*19*). An organics feature was not identified in the VIR global spectrum of Ceres (*1*). While the presence of organics cannot be excluded (*20*), we expect hydrogen is partitioned primarily between phyllosilicates and water ice on Ceres. The equatorial average [Fe] was determined to be 16 ± 1 wt.% from the Fe 7.6 MeV interaction rate and thermal + epithermal neutron measurements (*10*).

Aqueous alteration results in the separation of feed materials into a briny liquid and less mobile solid residue. Elements like Fe would be found primarily in the solid phase, whereas K and C are partially soluble and could be transported in the brine. The CI and CM chondrites underwent low-temperature aqueous processing, likely in a low permeability environment on a small parent body, where fluid flow was limited (*21*, *22*). This led to isochemical alteration (*8*). On larger bodies like Ceres, multi-km transport is possible, potentially resulting in ice-rock fractionation (*2*–*4*, *8*, *21*).

Analysis of the 1.461 MeV gamma ray produced by the decay of ^{40}K (*10*) gives an equatorial concentration for K of 410 ± 40 μg/g, intermediate between CI and CM averages, 550- and 370-μg/g, respectively (*23*); however, [K] depends on both nebular and parent-body processes (*24*). Without knowledge of Ceres' bulk [K], the regolith measurement is not diagnostic of chemical fractionation within Ceres. Carbon was detected by GRaND with a lower limit similar to carbonaceous chondrites (*10*).

If carbonaceous chondrite alteration were isochemical (*8*), the CI and CM chondrites should follow a water-dilution trend when [Fe] is plotted against WEH (Fig. 4). That [Fe] is lower than CI chondrites may result from differences in the bulk composition of the meteorite parent bodies and Ceres. Low regolith vapor diffusivity inferred by GRaND is consistent with small grains, which may be representative of primordial materials (*8*). Alternatively, internal processes, such as density-driven separation of Fe-rich phases from a primitive starting composition could explain the difference, while convective upwelling, possibly involving brines, could have led to the exposure of ice and fine grains on the surface (*4*). Coarse magnetite grains are found in CI and CM chondrites (*25*). Consequently, sedimentation could result in a surface depleted in Fe. Otherwise, Fe may be diluted by organic materials, carbonates or salts present in Ceres' crust (*7*, *10*, *26*). Systematic uncertainties may also contribute to differences between Ceres and the meteorites (Fig. 4).

Together, measurements of [Fe], [H], and [K] show that materials exposed on Ceres' surface have undergone aqueous processing. Evidence from GRaND for a fine-grained, C-bearing regolith, and differences between regolith [Fe] and [H] relative to CI chondrites, imply modest ice-rock fractionation. The high spatial uniformity of GRaND measurements of the ice-free, equatorial regolith indicates that ice-rock fractionation occurred on a global scale. The [H] within Ceres' icy regolith, about 27 wt.% WEH, is consistent with estimates of bulk H from Ceres' density (*1*, *2*). The ice table contains about 10 wt.% water ice, most likely sourced from endogenic liquid not consumed by alteration processes. The detection of widespread water ice at mid-to-high latitudes confirms predictions that ice can survive for billions of years within a meter of the surface.

REFERENCES AND NOTES

1. M. C. De Sanctis, E. Ammannito, A. Raponi, S. Marchi, T. B. McCord, H. Y. McSween, F. Capaccioni, M. T. Capria, F. G. Carrozzo, M. Ciarniello, A. Longobardo, F. Tosi, S. Fonte, M. Formisano, A. Frigeri, M. Giardino, G. Magni, E. Palomba, D. Turrini, F. Zambon, J.-P. Combe, W. Feldman, R. Jaumann, L. A. McFadden, C. M. Pieters, T. Prettyman, M. Toplis, C. A. Raymond, C. T. Russell, Ammoniated phyllosilicates with a likely outer solar system origin on (1) Ceres. *Nature* **528**, 241–244 (2015). doi:10.1038/nature16172 Medline
2. T. B. McCord, C. Sotin, Ceres: Evolution and current state. *J. Geophys. Res.* **110**, E05009 (2005). doi:10.1029/2004JE002244
3. J. C. Castillo-Rogez, T. B. McCord, Ceres' evolution and present state constrained by shape data. *Icarus* **205**, 443–459 (2010). doi:10.1016/j.icarus.2009.04.008
4. M. Neveu, S. J. Desch, Geochemistry, thermal evolution, and cryovolcanism on Ceres with a muddy ice mantle. *Geophys. Res. Lett.* **42**, 10197–10206 (2015). doi:10.1002/2015GL066375
5. J. P. Combe, T. B. McCord, F. Tosi, E. Ammannito, F. G. Carrozzo, M. C. De Sanctis, A. Raponi, S. Byrne, M. E. Landis, K. H. G. Hughson, C. A. Raymond, C. T. Russell, Detection of local H_2O exposed at the surface of Ceres. *Science* **353**, aaf3010 (2016). doi:10.1126/science.aaf3010 Medline
6. F. P. Fanale, J. R. Salvail, The water regime of asteroid (1) Ceres. *Icarus* **82**, 97–110 (1989). doi:10.1016/0019-1035(89)90026-2
7. R. S. Park, A. S. Konopliv, B. G. Bills, N. Rambaux, J. C. Castillo-Rogez, C. A. Raymond, A. T. Vaughan, A. I. Ermakov, M. T. Zuber, R. R. Fu, M. J. Toplis, C. T. Russell, A. Nathues, F. Preusker, A partially differentiated interior for (1) Ceres deduced from its gravity field and shape. *Nature* **537**, 515–517 (2016). doi:10.1038/nature18955 Medline
8. P. A. Bland, M. D. Jackson, R. F. Coker, B. A. Cohen, J. B. W. Webber, M. R. Lee, C. M. Duffy, R. J. Chater, M. G. Ardakani, D. S. McPhail, D. W. McComb, G. K. Benedix, Why aqueous alteration in asteroids was isochemical: High porosity ≠ high permeability. *Earth Planet. Sci. Lett.* **287**, 559–568 (2009). doi:10.1016/j.epsl.2009.09.004
9. T. H. Prettyman, W. C. Feldman, H. Y. McSween, R. D. Dingler, D. C. Enemark, D. E. Patrick, S. A. Storms, J. S. Hendricks, J. P. Morgenthaler, K. M. Pitman, R. C. Reedy, Dawn's gamma ray and neutron detector. *Space Sci. Rev.* **163**, 371–459 (2011). doi:10.1007/s11214-011-9862-0
10. See supplementary materials.
11. T. H. Prettyman, D. W. Mittlefehldt, N. Yamashita, D. J. Lawrence, A. W. Beck, W. C. Feldman, T. J. McCoy, H. Y. McSween, M. J. Toplis, T. N. Titus, P. Tricarico, R. C. Reedy, J. S. Hendricks, O. Forni, L. Le Corre, J.-Y. Li, H. Mizzon, V. Reddy, C. A. Raymond, C. T. Russell, Elemental mapping by Dawn reveals exogenic H in Vesta's regolith. *Science* **338**, 242–246 (2012). doi:10.1126/science.1225354 Medline
12. E. Ammannito, M. C. DeSanctis, M. Ciarniello, A. Frigeri, F. G. Carrozzo, J.-P. Combe, B. L. Ehlmann, S. Marchi, H. Y. McSween, A. Raponi, M. J. Toplis, F. Tosi, J. C. Castillo-Rogez, F. Capaccioni, M. T. Capria, S. Fonte, M. Giardino, R. Jaumann, A. Longobardo, S. P. Joy, G. Magni, T. B. McCord, L. A. McFadden, E. Palomba, C. M. Pieters, C. A. Polanskey, M. D. Rayman, C. A. Raymond, P. M. Schenk, F. Zambon, C. T. Russell, Distribution of phyllosilicates on the surface of Ceres. *Science* **353**, aaf4279 (2016). doi:10.1126/science.aaf4279 Medline
13. N. Schorghofer, Predictions of depth-to-ice on asteroids based on an asynchronous model of temperature, impact stirring, and ice loss. *Icarus* **276**, 88–95 (2016). doi:10.1016/j.icarus.2016.04.037

14. W. C. Feldman *et al.*, Global distribution of near-surface hydrogen on Mars. *J. Geophys. Res.* **109**, E09006 (2004). doi:10.1029/2003JE002160
15. D. T. Britt, G. J. S. J. Consolmagno, Stony meteorite porosities and densities: A review of data through 2001. *Meteorit. Planet. Sci.* **38**, 1161–1180 (2003). doi:10.1111/j.1945-5100.2003.tb00305.x
16. M. Küppers, L. O'Rourke, D. Bockelée-Morvan, V. Zakharov, S. Lee, P. von Allmen, B. Carry, D. Teyssier, A. Marston, T. Müller, J. Crovisier, M. A. Barucci, R. Moreno, Localized sources of water vapour on the dwarf planet (1) Ceres. *Nature* **505**, 525–527 (2014). doi:10.1038/nature12918 Medline
17. C. T. Russell, C. A. Raymond, E. Ammannito, D. L. Buczkowski, M. C. De Sanctis, H. Hiesinger, R. Jaumann, A. S. Konopliv, H. Y. McSween, A. Nathues, R. S. Park, C. M. Pieters, T. H. Prettyman, T. B. McCord, L. A. McFadden, S. Mottola, M. T. Zuber, S. P. Joy, C. Polanskey, M. D. Rayman, J. C. Castillo-Rogez, P. J. Chi, J. P. Combe, A. Ermakov, R. R. Fu, M. Hoffmann, Y. D. Jia, S. D. King, D. J. Lawrence, J.-Y. Li, S. Marchi, F. Preusker, T. Roatsch, O. Ruesch, P. Schenk, M. N. Villarreal, N. Yamashita, Dawn arrives at Ceres: Exploration of a small, volatile-rich world. *Science* **353**, 1008–1010 (2016). doi:10.1126/science.aaf4219 Medline
18. C. M. O'D. Alexander, R. Bowden, M. L. Fogel, K. T. Howard, C. D. K. Herd, L. R. Nittler, The provenances of asteroids, and their contributions to the volatile inventories of the terrestrial planets. *Science* **337**, 721–723 (2012). doi:10.1126/science.1223474 Medline
19. S. Derenne, F. Robert, Model of molecular structure of the insoluble organic matter isolated from Murchison meteorite. *Meteorit. Planet. Sci.* **45**, 1461–1475 (2010). doi:10.1111/j.1945-5100.2010.01122.x
20. A. Garenne, P. Beck, G. Montes-Hernandez, O. Brissaud, B. Schmitt, E. Quirico, L. Bonal, C. Beck, K. T. Howard, Bidirectional reflectance spectroscopy of carbonaceous chondrites: Implications for water quantification and primary composition. *Icarus* **264**, 172–183 (2016). doi:10.1016/j.icarus.2015.09.005
21. E. D. Young, K. K. Zhang, G. Schubert, Conditions for pore water convection within carbonaceous chondrite parent bodies – implications for planetesimal size and heat production. *Earth Planet. Sci. Lett.* **213**, 249–259 (2003). doi:10.1016/S0012-821X(03)00345-5
22. A. J. Brearley, Nebular versus parent-body processing. *Treatise on Geochemistry* **1**, 711 (2003).
23. K. Lodders, B. Fegley Jr., *The Planetary Scientist's Companion* (Oxford University Press on Demand, 1998).
24. M. Humayun, R. N. Clayton, Potassium isotope cosmochemistry: Genetic implications of volatile element depletion. *Geochim. Cosmochim. Acta* **59**, 2131–2148 (1995). doi:10.1016/0016-7037(95)00132-8
25. H. Y. McSween Jr., S. M. Richardson, The composition of carbonaceous chondrite matrix. *Geochim. Cosmochim. Acta* **41**, 1145–1161 (1977). doi:10.1016/0016-7037(77)90110-7
26. M. C. De Sanctis, A. Raponi, E. Ammannito, M. Ciarniello, M. J. Toplis, H. Y. McSween, J. C. Castillo-Rogez, B. L. Ehlmann, F. G. Carrozzo, S. Marchi, F. Tosi, F. Zambon, F. Capaccioni, M. T. Capria, S. Fonte, M. Formisano, A. Frigeri, M. Giardino, A. Longobardo, G. Magni, E. Palomba, L. A. McFadden, C. M. Pieters, R. Jaumann, P. Schenk, R. Mugnuolo, C. A. Raymond, C. T. Russell, Bright carbonate deposits as evidence of aqueous alteration on (1) Ceres. *Nature* **536**, 54–57 (2016). doi:10.1038/nature18290 Medline
27. W. C. Feldman *et al.*, Gamma-ray, neutron, and alpha-particle spectrometers for the Lunar Prospector mission. *J. Geophys. Res.* **109**, E07S06 (2004). doi:10.1029/2003JE002207
28. G. F. Knoll, *Radiation Detection and Measurement* (John Wiley & Sons, Inc., 1989).
29. T. H. Prettyman, "Dawn Gamma Ray and Neutron Detector raw Ceres counts V1.0," *DAWN-A-GRAND-2-EDR-CERES-COUNTS-V1.0*, https://pds.jpl.nasa.gov (NASA Planetary Data System, 2016).
30. T. H. Prettyman, N. Yamashita, "Dawn Gamma Ray and Neutron Detector calibrated Ceres counts V1.0," *DAWN-A-GRAND-3-RDR-CERES-COUNTS-V1.0*, https://pds.jpl.nasa.gov (NASA Planetary Data System, 2016).
31. D. J. Lawrence, P. N. Peplowski, T. H. Prettyman, W. C. Feldman, D. Bazell, D. W. Mittlefehldt, R. C. Reedy, N. Yamashita, Constraints on Vesta's elemental composition: Fast neutron measurements by Dawn's gamma ray and neutron detector. *Meteorit. Planet. Sci.* **48**, 2271–2288 (2013). doi:10.1111/maps.12187 Medline
32. N. Yamashita, T. H. Prettyman, D. W. Mittlefehldt, M. J. Toplis, T. J. McCoy, A. W. Beck, R. C. Reedy, W. C. Feldman, D. J. Lawrence, P. N. Peplowski, O. Forni, H. Mizzon, C. A. Raymond, C. T. Russell, Distribution of iron on Vesta. *Meteorit. Planet. Sci.* **48**, 2237–2251 (2013). doi:10.1111/maps.12139
33. T. H. Prettyman *et al.*, Composition and structure of the martian surface at high southern latitudes from neutron spectroscopy. *J. Geophys. Res.* **109**, E05001 (2004). doi:10.1029/2003JE002139
34. D. B. Pelowitz, (Ed.), MCNPX User's Manual, Los Alamos National Laboratory document LA-CP-11-00438 (2011).
35. G. W. McKinney, D. J. Lawrence, T. H. Prettyman, R. C. Elphic, W. C. Feldman, J. J. Hagerty, MCNPX benchmark for cosmic ray interactions with the Moon. *J. Geophys. Res.* **111**, E06004 (2006). doi:10.1029/2005JE002551
36. Radiation Safety Information Computational Center (RSICC), Oak Ridge National Laboratory, https://rsicc.ornl.gov/.
37. I. G. Mitrofanov, M. T. Zuber, M. L. Litvak, W. V. Boynton, D. E. Smith, D. Drake, D. Hamara, A. S. Kozyrev, A. B. Sanin, C. Shinohara, R. S. Saunders, V. Tretyakov, CO_2 snow depth and subsurface water-ice abundance in the northern hemisphere of Mars. *Science* **300**, 2081–2084 (2003). doi:10.1126/science.1084350 Medline
38. W. V. Boynton, G. J. Taylor, L. G. Evans, R. C. Reedy, R. Starr, D. M. Janes, K. E. Kerry, D. M. Drake, K. J. Kim, R. M. S. Williams, M. K. Crombie, J. M. Dohm, V. Baker, A. E. Metzger, S. Karunatillake, J. M. Keller, H. E. Newsom, J. R. Arnold, J. Brückner, P. A. J. Englert, O. Gasnault, A. L. Sprague, I. Mitrofanov, S. W. Squyres, J. I. Trombka, L. d'Uston, H. Wänke, D. K. Hamara, Concentration of H, Si, Cl, K, Fe, and Th in the low- and mid-latitude regions of Mars. *J. Geophys. Res.* **112**, E12S99 (2007). doi:10.1029/2007JE002887
39. D. J. Lawrence, W. C. Feldman, J. O. Goldsten, S. Maurice, P. N. Peplowski, B. J. Anderson, D. Bazell, R. L. McNutt Jr., L. R. Nittler, T. H. Prettyman, D. J. Rodgers, S. C. Solomon, S. Z. Weider, Evidence for water ice near Mercury's north pole from MESSENGER Neutron Spectrometer measurements. *Science* **339**, 292–296 (2013). doi:10.1126/science.1229953 Medline
40. T. H. Prettyman, D. W. Mittlefehldt, N. Yamashita, A. W. Beck, W. C. Feldman, J. S. Hendricks, D. J. Lawrence, T. J. McCoy, H. Y. McSween, P. N. Peplowski, R. C. Reedy, M. J. Toplis, L. Le Corre, H. Mizzon, V. Reddy, T. N. Titus, C. A. Raymond, C. T. Russell, Neutron absorption constraints on the composition of 4 Vesta. *Meteorit. Planet. Sci.* **48**, 2211–2236 (2013). doi:10.1111/maps.12244
41. P. M. O'Neill, Badhwar–O'Neill 2010 galactic cosmic ray flux model—revised. *IEEE Trans. Nucl. Sci.* **6**, 3148–3153 (2010).
42. The Badhwar and O'Neill Galactic Cosmic Ray (GCR) model can be obtained by sending a request to patrick.m.oneill@nasa.gov.
43. T. H. Prettyman, "Dawn GRaND Ephemeris, Pointing, and Geometry, V2," *DAWN-A-GRAND-3-RDR-CERES-COUNTS-V1.0*, https://pds.jpl.nasa.gov (NASA Planetary Data System, 2016).
44. R. P. Gardner, K. Verghese, On the solid angle subtended by a circular disk. *Nucl. Instrum. Methods* **93**, 163–167 (1971). doi:10.1016/0029-554X(71)90155-8
45. M. H. Kalos, P. A. Whitlock, *Monte Carlo Methods, Volume I: Basics* (John Wiley & Sons, Inc., 1986).
46. D. W. Mittlefehldt, Asteroid (4) Vesta: I. The howardite-eucrite-diogenite (HED) clan of meteorites. *Chemie der Erde - Geochemistry* **75**, 155–183 (2015). doi:10.1016/j.chemer.2014.08.002
47. E. K. Jessberger, A. Christoforidis, J. Kissel, Aspects of the major element composition of Halley's dust. *Nature* **332**, 691–695 (1988). doi:10.1038/332691a0
48. W. C. Feldman, A. Pathare, S. Maurice, T. H. Prettyman, D. J. Lawrence, R. E. Milliken, B. J. Travis, Mars Odyssey neutron data: 2. Search for buried excess water ice deposits at nonpolar latitudes on Mars. *J. Geophys. Res.* **116**, E11009 (2011). doi:10.1029/2011JE003806
49. A. S. Rivkin, J.-Y. Li, R. E. Milliken, L. F. Lim, A. J. Lovell, B. E. Schmidt, L. A. McFadden, B. A. Cohen, The surface composition of Ceres. *Space Sci. Rev.* **163**, 95–116 (2010). doi:10.1007/s11214-010-9677-4
50. T. N. Titus, Ceres: Predictions for near-surface water ice stability and implications for plume generating processes. *Geophys. Res. Lett.* **42**, 2130–2136 (2015). doi:10.1002/2015GL063240
51. P. O. Hayne, O. Aharonson, Thermal stability of ice on Ceres with rough topography. *J. Geophys. Res. Planets* **120**, 1567–1584 (2015).

doi:10.1002/2015JE004887
52. AstDyS-2 Asteroids Dynamic Site, http://hamilton.dm.unipi.it/astdys/index.php?pc=1.1.6&n=1, Retrieved 3 November 2016.
53. N. Schorghofer, The lifetime of ice on main belt asteroids. *Astrophys. J.* **682**, 697–705 (2008). doi:10.1086/588633
54. N. Schorghofer, Planetary-code-collection: Thermal and ice evolution models for planetary surfaces v1.1.1; https://github.com/nschorgh/Planetary-Code-Collection/; doi:10.5281/zenodo.48851 (2016).
55. A. W. Beck, D. J. Lawrence, P. N. Peplowski, T. H. Prettyman, T. J. McCoy, H. Y. McSween Jr., M. J. Toplis, N. Yamashita, Using HED meteorites to interpret neutron and gamma-ray data from asteroid 4 Vesta. *Meteorit. Planet. Sci.* **50**, 1311–1337 (2015). doi:10.1111/maps.12467
56. J. A. Cartwright, U. Ott, D. W. Mittlefehldt, J. S. Herrin, S. Herrmann, S. A. Mertzman, K. R. Mertzman, Z. X. Peng, J. E. Quinn, The quest for regolithic howardites. Part 1: Two trends uncovered using noble gases. *Geochim. Cosmochim. Acta* **105**, 395–421 (2013). doi:10.1016/j.gca.2012.11.047
57. J. A. Cartwright, U. Ott, D. W. Mittlefehldt, The quest for regolithic howardites. Part 2: Surface origins highlighted by noble gases. *Geochim. Cosmochim. Acta* **140**, 488–508 (2014). doi:10.1016/j.gca.2014.05.033
58. N. G. Lunning, K. C. Welten, H. Y. McSween Jr., M. W. Caffee, A. W. Beck, Grosvenor Mountains 95 howardite pairing group: Insights into the surface regolith of asteroid 4 Vesta. *Meteorit. Planet. Sci.* **51**, 167–194 (2016). doi:10.1111/maps.12580
59. R. Jaumann, D. A. Williams, D. L. Buczkowski, R. A. Yingst, F. Preusker, H. Hiesinger, N. Schmedemann, T. Kneissl, J. B. Vincent, D. T. Blewett, B. J. Buratti, U. Carsenty, B. W. Denevi, M. C. De Sanctis, W. B. Garry, H. U. Keller, E. Kersten, K. Krohn, J.-Y. Li, S. Marchi, K. D. Matz, T. B. McCord, H. Y. McSween, S. C. Mest, D. W. Mittlefehldt, S. Mottola, A. Nathues, G. Neukum, D. P. O'Brien, C. M. Pieters, T. H. Prettyman, C. A. Raymond, T. Roatsch, C. T. Russell, P. Schenk, B. E. Schmidt, F. Scholten, K. Stephan, M. V. Sykes, P. Tricarico, R. Wagner, M. T. Zuber, H. Sierks, Vesta's shape and morphology. *Science* **336**, 687–690 (2012). doi:10.1126/science.1219122 Medline
60. P. Schenk, D. P. O'Brien, S. Marchi, R. Gaskell, F. Preusker, T. Roatsch, R. Jaumann, D. Buczkowski, T. McCord, H. Y. McSween, D. Williams, A. Yingst, C. Raymond, C. Russell, The geologically recent giant impact basins at Vesta's south pole. *Science* **336**, 694–697 (2012). doi:10.1126/science.1223272 Medline
61. M. C. De Sanctis, J.-P. Combe, E. Ammannito, E. Palomba, A. Longobardo, T. B. McCord, S. Marchi, F. Capaccioni, M. T. Capria, D. W. Mittlefehldt, C. M. Pieters, J. Sunshine, F. Tosi, F. Zambon, F. Carraro, S. Fonte, A. Frigeri, G. Magni, C. A. Raymond, C. T. Russell, D. Turrini, Detection of widespread hydrated materials on Vesta by the VIR imaging spectrometer on board the Dawn mission. *Astrophys. J.* **758**, L36 (2012). doi:10.1088/2041-8205/758/2/L36
62. E. Fermi, *Nuclear Physics: A course given by Enrico Fermi at the University of Chicago. Notes compiled by Jay Orear, A. H. Rosenfeld, and R. A. Schluter* (The University of Chicago Press, Chicago, Illinois, ed. Revised Edition, 1950).
63. P. N. Peplowski, R. L. Klima, D. J. Lawrence, C. M. Ernst, B. W. Denevi, E. A. Frank, J. O. Goldsten, S. L. Murchie, L. R. Nittler, S. C. Solomon, Remote sensing evidence for an ancient carbon-bearing crust on Mercury. *Nat. Geosci.* **9**, 273–276 (2016). doi:10.1038/ngeo2669
64. R. C. Little, Latitude variation of the subsurface lunar temperature: Lunar Prospector thermal neutrons. *J. Geophys. Res.* **108**, 5046 (2003). doi:10.1029/2001JE001497
65. N. Yamashita, T. H. Prettyman, "Dawn's Gamma Ray and Neutron Detector: BGO Data Processing, Version 4.1," *DAWN-A-GRAND-3-RDR-CERES-COUNTS-V1.0*, https://pds.jpl.nasa.gov (NASA Planetary Data System, 2016).
66. R. C. Reedy, Planetary gamma-ray spectroscopy. *9th Lunar Planet. Sci. Conf.*, 2961-2984 (1978).
67. T. H. Prettyman, N. Yamashita, R. C. Reedy, H. Y. McSween Jr., D. W. Mittlefehldt, J. S. Hendricks, M. J. Toplis, Concentrations of potassium and thorium within Vesta's regolith. *Icarus* **259**, 39–52 (2015). doi:10.1016/j.icarus.2015.05.035
68. XCOM, Photon cross sections database, National Institute of Standards and Technology; http://physics.nist.gov/PhysRefData/Xcom/html/xcom1.html; Retrieved on 3 November 2016.
69. P. N. Peplowski, D. J. Lawrence, L. G. Evans, R. L. Klima, D. T. Blewett, J. O. Goldsten, S. L. Murchie, T. J. McCoy, L. R. Nittler, S. C. Solomon, R. D. Starr, S. Z. Weider, Constraints on the abundance of carbon in near-surface materials on Mercury: Results from the MESSENGER Gamma-Ray Spectrometer. *Planet. Space Sci.* **108**, 98–107 (2015). doi:10.1016/j.pss.2015.01.008
70. T. H. Prettyman, J. J. Hagerty, R. C. Elphic, W. C. Feldman, D. J. Lawrence, G. W. McKinney, D. T. Vaniman, Elemental composition of the lunar surface: Analysis of gamma ray spectroscopy data from Lunar Prospector. *J. Geophys. Res.* **111**, E12007 (2006). doi:10.1029/2005JE002656
71. C. M. O'D. Alexander, K. T. Howard, R. Bowden, M. L. Fogel, The classification of CM and CR chondrites using bulk H, C and N abundances and isotopic compositions. *Geochim. Cosmochim. Acta* **123**, 244–260 (2013). doi:10.1016/j.gca.2013.05.019
72. A. Garenne, P. Beck, G. Montes-Hernandez, R. Chiriac, F. Toche, E. Quirico, L. Bonal, B. Schmitt, The abundance and stability of "water" in type 1 and 2 carbonaceous chondrites (CI, CM and CR). *Geochim. Cosmochim. Acta* **137**, 93–112 (2014). doi:10.1016/j.gca.2014.03.034
73. A. J. King, J. R. Solomon, P. F. Schofield, S. S. Russell, Characterising the CI and CI-like carbonaceous chondrites using thermogravimetric analysis and infrared spectroscopy. *Earth Planets Space* **67**, 198 (2015). doi:10.1186/s40623-015-0370-4
74. A. E. Rubin, Mineralogy of meteorite groups. *Meteorit. Planet. Sci.* **32**, 231–247 (1997). doi:10.1111/j.1945-5100.1997.tb01262.x
75. K. Tomeoka, P. R. Buseck, Matrix mineralogy of the Orgueil CI carbonaceous chondrite. *Geochim. Cosmochim. Acta* **52**, 1627–1640 (1988). doi:10.1016/0016-7037(88)90231-1
76. A. P. Zent, D. J. Howard, R. C. Quinn, H_2O adsorption on smectites: Application to the diurnal variation of H_2O in the Martian atmosphere. *J. Geophys. Res. Planets* **106**, 14667–14674 (2001). doi:10.1029/2000JE001394
77. T. B. McCord, T. M. Orlando, G. Teeter, G. B. Hansen, M. T. Sieger, N. G. Petrik, L. Van Keulen, Thermal and radiation stability of the hydrated salt minerals epsomite, mirabilite, and natron under Europa environmental conditions. *J. Geophys. Res. Planets* **106**, 3311–3319 (2001). doi:10.1029/2000JE001282
78. C. M. O'D. Alexander, R. Bowden, M. L. Fogel, K. T. Howard, Carbonate abundances and isotopic compositions in chondrites. *Meteorit. Planet. Sci.* **50**, 810–833 (2015). doi:10.1111/maps.12410
79. A. R. Hendrix, F. Vilas, J.-Y. Li, The UV signature of carbon in the solar system. *Meteorit. Planet. Sci.* **51**, 105–115 (2016). doi:10.1111/maps.12575
80. E. J. Zeller, L. B. Ronca, Space weathering of lunar and asteroidal surfaces. *Icarus* **7**, 372–379 (1967). doi:10.1016/0019-1035(67)90082-6
81. S. Marchi, A. I. Ermakov, C. A. Raymond, R. R. Fu, D. P. O'Brien, M. T. Bland, E. Ammannito, M. C. De Sanctis, T. Bowling, P. Schenk, J. E. C. Scully, D. L. Buczkowski, D. A. Williams, H. Hiesinger, C. T. Russell, The missing large impact craters on Ceres. *Nat. Commun.* **7**, 12257 (2016). doi:10.1038/ncomms12257 Medline
82. R. T. Daly, P. H. Schultz, Predictions for impactor contamination on Ceres based on hypervelocity impact experiments. *Geophys. Res. Lett.* **42**, 7890–7898 (2015). doi:10.1002/2015GL065601
83. W. C. Feldman, D. J. Lawrence, R. C. Elphic, D. T. Vaniman, D. R. Thomsen, B. L. Barraclough, S. Maurice, A. B. Binder, Chemical information content of lunar thermal and epithermal neutrons. *J. Geophys. Res.* **105**, 20347–20363 (2000). doi:10.1029/1999JE001183
84. D. Wolf, H. Palme, The solar system abundances of phosphorus and titanium and the nebular volatility of phosphorus. *Meteorit. Planet. Sci.* **36**, 559–571 (2001). doi:10.1111/j.1945-5100.2001.tb01897.x
85. E. Jarosewich, Chemical analyses of meteorites at the Smithsonian Institution: An update. *Meteorit. Planet. Sci.* **41**, 1381–1382 (2006). doi:10.1111/j.1945-5100.2006.tb00528.x
86. A. E. Rubin, J. M. Trigo-Rodríguez, H. Huber, J. T. Wasson, Progressive aqueous alteration of CM carbonaceous chondrites. *Geochim. Cosmochim. Acta* **71**, 2361–2382 (2007). doi:10.1016/j.gca.2007.02.008
87. E. Jarosewich, Chemical analyses of meteorites: A compilation of stony and iron meteorite analyses. *Meteoritics* **25**, 323–337 (1990). doi:10.1111/j.1945-5100.1990.tb00717.x
88. H. B. Wiik, On regular discontinuities in the composition of meteorites. *Societas Scientarium Fennica. Comment. Phys.-Math.* **34**, 135–145 (1969).

89. H. B. Wiik, The chemical composition of some stony meteorites. *Geochim. Cosmochim. Acta* **9**, 279–289 (1956). doi:10.1016/0016-7037(56)90028-X

ACKNOWLEDGMENTS

Portions of this work were performed by the Planetary Science Institute under contract with the Jet Propulsion Laboratory, California Institute of Technology (JPL); by JPL under contract with NASA; and by the NASA Dawn at Ceres Guest Investigator Program. The Dawn mission is led by the University of California, Los Angeles, and managed by JPL under the auspices of the NASA Discovery Program Office. The Dawn data are archived with the NASA Planetary Data System (http://sbn.psi.edu/pds/archive/dawn.html).

SUPPLEMENTARY MATERIALS

www.sciencemag.org/cgi/content/full/science.aah6765/DC1
Materials and Methods
Supplementary Text
Figs. S1 to S18
Tables S1 to S4
References (*27–89*)

31 July 2016; accepted 23 November 2016
Published online 15 December 2016
10.1126/science.aah6765

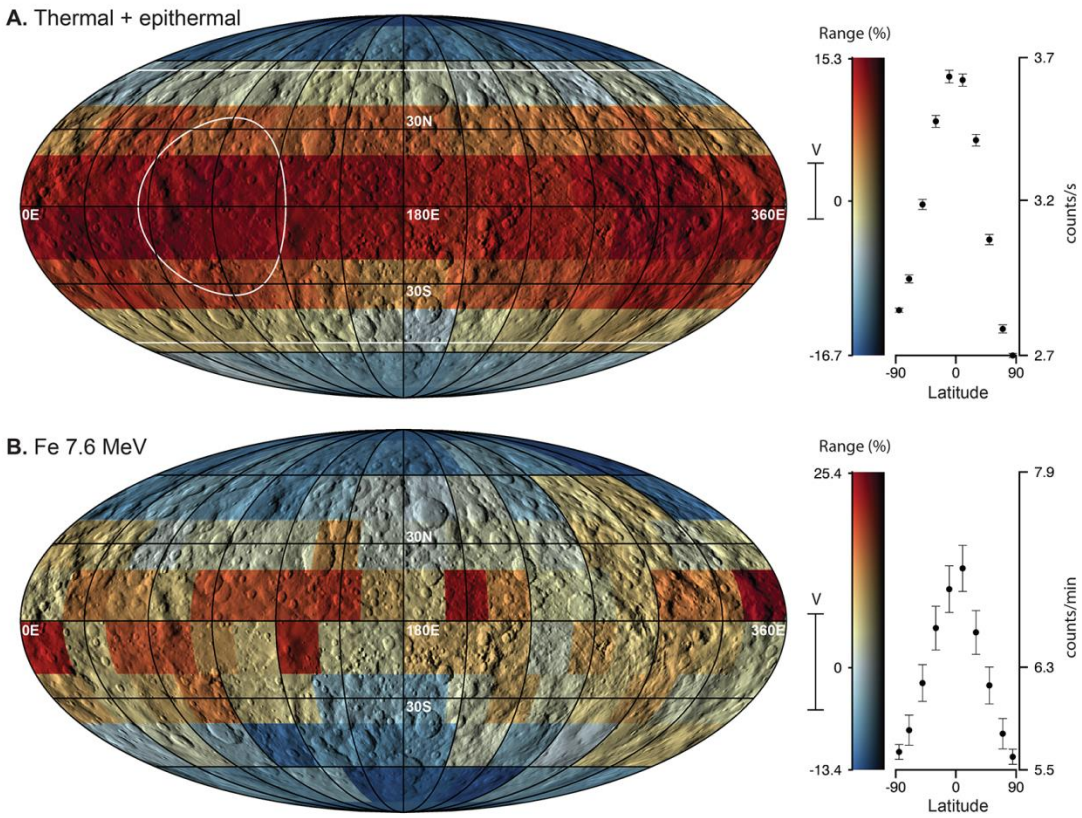

Fig. 1. Maps of corrected neutron and gamma ray counting rates from data acquired at low altitude. (**A**) ^{6}Li(n,α) reaction rate in lithium-loaded glass (thermal + epithermal neutrons); (**B**) Full energy interaction rate of 7.6 MeV Fe capture gamma rays in bismuth germanate. East longitude convention is used (*17*) and data are superimposed on shaded relief. The white circle indicates the approximate full-width-at-half-maximum (FWHM) spatial resolution at a selected equatorial measurement location. The white lines indicate the FWHM at the poles. The absolute rate and dynamic range are shown along with rates averaged over latitude bands (zonal averages) and average pixel uncertainties (1-sigma error bars). The dynamic range for the same measurements at Vesta is shown for comparison (V).

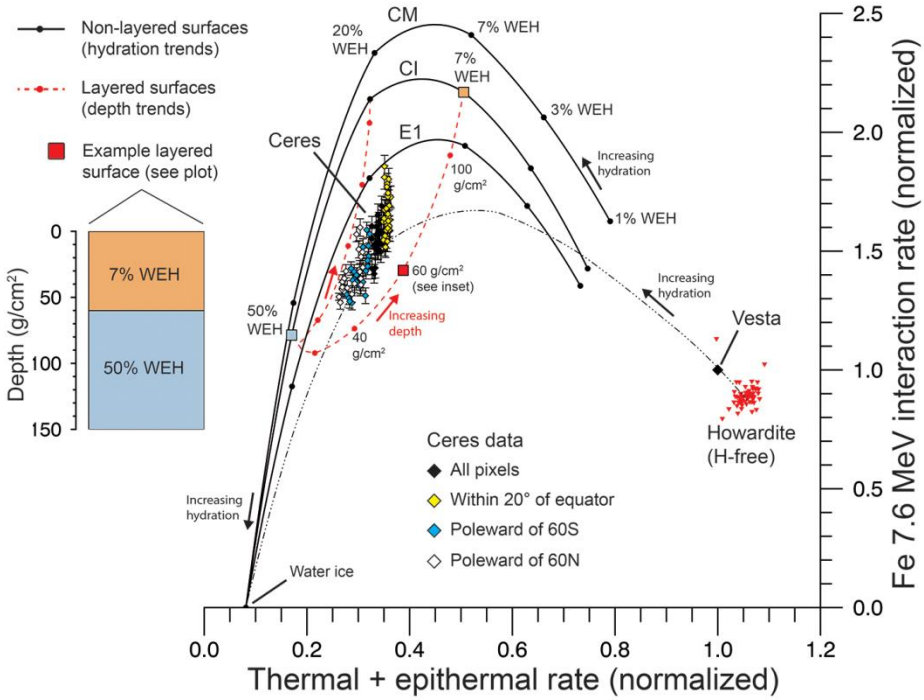

Fig. 2. Comparison of mapped data with model compositions. Data from Fig. 1 are compared with Vesta's global average and selected model compositions, including CI/CM chondrite meteorites (*23*), simulated material E1 (*10*) with lower average [Fe] and higher [C] than meteorite analogs (brackets indicate concentration). Solid curves show the variation of counts with [H] (1- to 100-wt.% WEH) for non-layered surfaces. Dashed red lines indicate example trends for layered surfaces. Selected points are labeled with depth in mass units (g/cm^2), given by the product of depth (cm) and regolith density (g/cm^3).

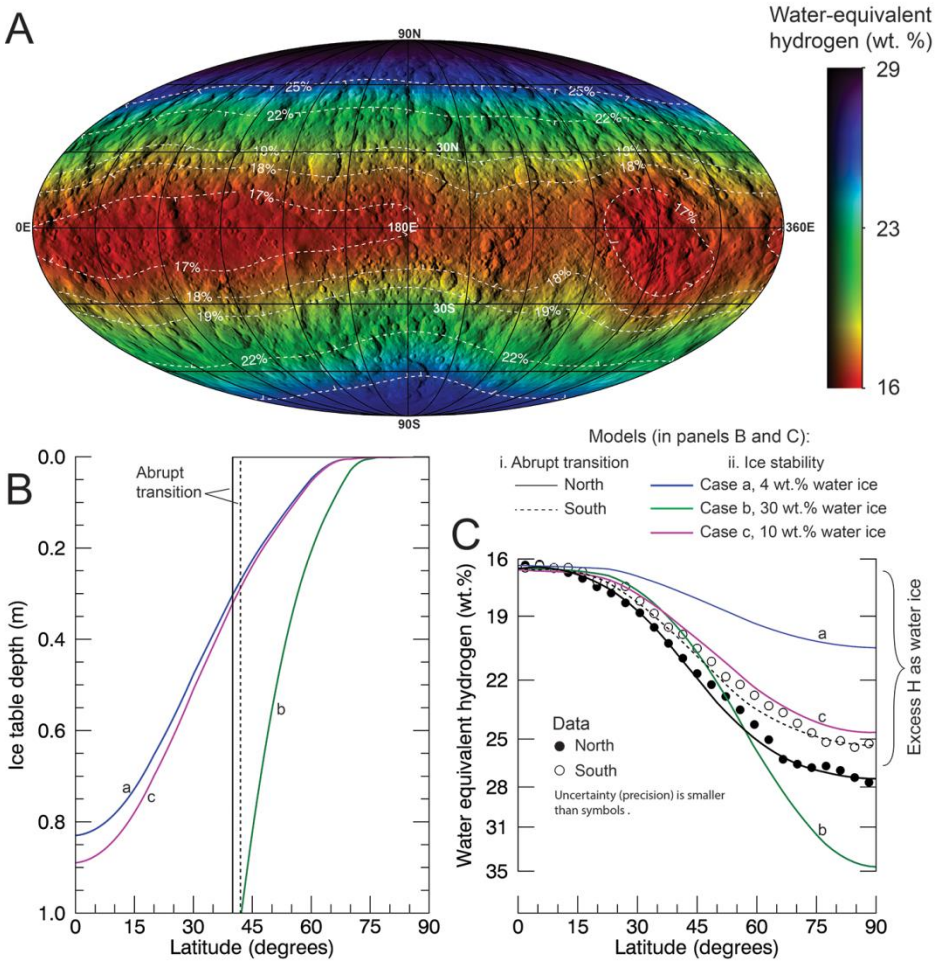

Fig. 3. Distribution of hydrogen and comparison with ice stability models. (**A**) The distribution of hydrogen (lower bound) within Ceres' regolith determined from thermal + epithermal neutron counting data. (**B**) Trial distributions of ice table depth with latitude: (i) A step function for which ice is at depths much greater than a meter at the equator and transitions abruptly to the surface at higher latitudes; (ii) Ice table depths determined by an ice stability model (*10*, *13*) for three cases corresponding to different vapor diffusivities and pore-filling ice content: (a) low diffusivity, with a grain size of 1 μm and porosity of 0.1 (4 wt.% water ice); (b) high diffusivity, with a grain size of 10 μm and porosity of 0.5 (30 wt.% water ice); (c) low diffusivity, with a grain size of 1 μm and porosity of 0.2 (10 wt.% water ice). (**C**) Forward models of thermal + epithermal counting rates (*10*) for each trial distribution are compared to zonally-averaged counting data, displayed in terms of water equivalent hydrogen for both hemispheres. For the step functions, the transition latitude and polar water ice content were adjusted to fit the data.

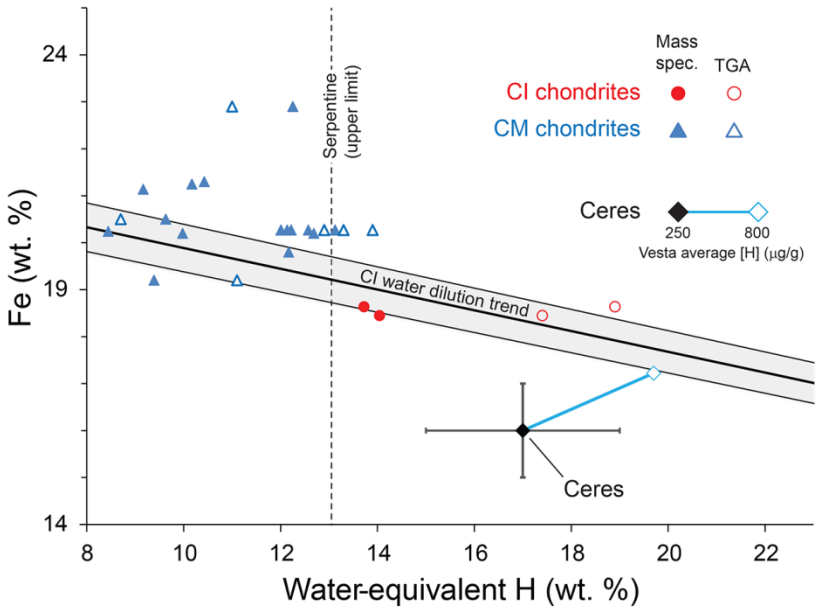

Fig. 4. Fe versus water-equivalent H for the CI and CM chondrites and Ceres. Recent measurements of H via mass spectrometry and thermogravimetric analysis (TGA) are shown. See (*10*) for data sources. Water dilution trends, in which [Fe] is adjusted by adding or removing water, are displayed for the CI chondrites (brackets denote concentration). Ceres equatorial average is shown as a point with error bars. The decrease in Fe on Ceres relative to the CI chondrite trend is consistent with the addition of 13 wt.% of a neutral component. The analysis assumes the minimum for the average [H] on Vesta of (250 μg/g). Increasing the hydrogen content of Vesta's regolith causes Ceres' regolith composition to shift toward the dilution trend for CI chondrites. Ceres pristine regolith would have lower [Fe] and higher [H] if the regolith contained significant exogenic contamination (*10*).

Extensive water ice within Ceres' aqueously altered regolith: Evidence from nuclear spectroscopy

T. H. Prettyman, N. Yamashita, M. J. Toplis, H. Y. McSween, N. Schorghofer, S. Marchi, W. C. Feldman, J. Castillo-Rogez, O. Forni, D. J. Lawrence, E. Ammannito, B. L. Ehlmann, H. G. Sizemore, S. P. Joy, C. A. Polanskey, M. D. Rayman, C. A. Raymond and C. T. Russell

(December 15, 2016)
published online December 15, 2016

Editor's Summary